

Spinning a levitated mechanical oscillator far into the deep-strong coupling regime

J. A. Zielińska,^{1,*} F. van der Laan,^{1,2} A. Norrman,^{1,3} R. Reimann,^{1,4} M. Frimmer,¹ and L. Novotny¹

¹Photonics Laboratory, ETH Zürich, CH-8093 Zürich, Switzerland

²Center for Nanophotonics, AMOLF, 1098 XG Amsterdam, The Netherlands

³Center for Photonics Sciences, University of Eastern Finland, P.O. Box 111, FI-80101 Joensuu, Finland

⁴Quantum Research Center, Technology Innovation Institute, Abu Dhabi, UAE

The field of levitodynamics has made substantial advancements in manipulating the translational and rotational degrees of freedom of levitated nanoparticles. Notably, rotational degrees of freedom can now be cooled to millikelvin temperatures and driven into GHz rotational speeds. However, in the case of cylindrically symmetric nanorotors, only the rotations around their short axes have been effectively manipulated, while the possibility to control rotation around the longer axis has remained a notable gap in the field. Here, we extend the rotational control toolbox by engineering an optically levitated nanodumbbell in vacuum into controlled spinning around its long axis with spinning rates exceeding 1 GHz. This fast spinning introduces deep-strong coupling between the nanodumbbell's libration modes, such that the coupling rate g exceeds the bare libration frequencies Ω_0 by two orders of magnitude with $g/\Omega_0 = 724 \pm 33$. Our control over the long-axis rotation opens the door to study the physics of deep-strong coupled mechanical oscillators and to observe macroscopic rotational quantum interference effects, thus laying a solid foundation for future applications in quantum technologies. Additionally, we find that our system offers great potential as a nanoscopic gyroscope with competitive sensitivity.

INTRODUCTION.

Cylindrically symmetric nanorotors, when trapped within linearly polarized optical tweezers, align their most polarizable (long) axis to the polarization direction of the tweezers. This results in the emergence of two degenerate libration modes corresponding to oscillatory rotations around the two least-polarizable (short) axes. Recently, significant advances have been made in controlling the short axis rotations, with nanorotors being driven to spin at GHz rates [1–4], libration oscillations cooled down to mK temperatures [5–8], and numerous demonstrations of torque sensing [3, 9–12]. However, the remaining rotational degree of freedom, which involves the nanoparticle's rotation around its long axis, typically remains unconstrained and is driven by thermal fluctuations [5, 6, 13]. Introducing controlled long axis spinning as a tool within rotational levitodynamics would enable the study of deep-strong coupling between mechanical modes, open up an avenue towards engineered quantum rotational dynamics [14], and significantly improve real-world technological prospects of nanoscopic levitated gyroscopes.

The generation of strongly and ultrastrongly coupled states is an ongoing experimental effort of the levitodynamics community [15–18], as it paves the way towards non-Hermitian dynamics [19] and entanglement generation [20]. The deep-strong coupling regime is reached when the coupling rate of two modes g dominates over all other system dynamics, including the eigenfrequencies of the uncoupled system. However, reaching such strong coupling is not trivial since it can result in unstable

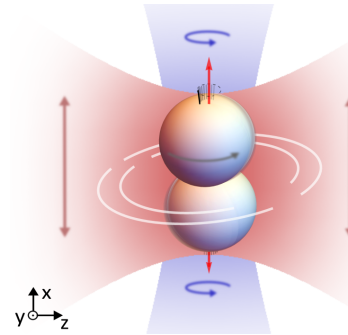


Figure 1. A nanodumbbell (not to scale) is trapped by an x polarized laser beam (red) and spun around its long axis by a circularly polarized spinning beam (blue).

dynamics [18, 21]. Interestingly, we find that the deep-strong coupling regime can be readily reached for the libration modes of a cylindrically symmetric rotor. Here, the coupling rate is proportional to the long-axis spinning frequency, which can be made arbitrarily large without running into mechanical instabilities. We reach coupling strengths g that are a factor of 724 larger than the uncoupled libration frequencies Ω_0 , outperforming the g/Ω_0 values demonstrated with trapped atoms by a large margin [22].

One of the main objectives of rotational levitodynamics is to probe quantum interference in the orientational dynamics of nanorotors, which have no analogue in the centre-of-mass motion of the object and no correspondence in classical physics [14]. The angular momentum of a free quantum rotor, e.g., a molecule, is quantized and in principle it can be prepared in a single eigenstate [23]. Unlike librational modes, which are governed by harmonic dynamics, the spinning around the long axis defines a *free rotational* degree of freedom

* jzielinska@eth.ch

and its corresponding angular momentum component is quantized. Controlling long-axis spinning while simultaneously manipulating (e.g. by feedback cooling) and detecting the remaining two angular directions allows to create a state with a large main angular momentum component. This in turn paves the way towards observing angular momentum quantization on a macroscopic scale and eventually engineering a nanorotor in a well-defined angular momentum quantum state. What is more, exploring the interaction between rotations around the long axis and light is a notable experimental and theoretical gap in the field. Understanding the resulting decoherence of nanorotors is crucial for the exploration of quantum rotational effects [14], such as rotational revivals [24] or rotational quantum non-demolition measurements [25].

Finally, fast-spinning levitated nanoparticles also offer significant advantages for inertial sensing of rotations. These objects, isolated from the surrounding environment, can be controlled down to their fundamental quantum and thermodynamic limits [4, 6]. However, for gyroscope applications, it is essential to achieve efficient detection of the spinning axis orientation, which is not feasible when the particle spins around its short axis [26]. Consequently, to fully explore the advantages of levitated nanoparticles for inertial sensing, it is vital to attain controlled rotation around the long axis.

In this work, we experimentally realize controlled rotation of a nanodumbbell around its long axis. The rotation rate, reaching over a GHz, is inferred from the coupling it creates between the two libration degrees of freedom. This coupling reaches far into the deep-strong coupling regime with $g/\Omega_0 = 724 \pm 33$.

SYSTEM UNDER STUDY.

Our system, illustrated in Fig. 1, consists of an optically levitated nanodumbbell exposed to a light field in a three-dimensional (3D) polarization state [27, 28]. The light field is composed of two parts: a strong tweezers field, linearly polarized along the x axis and propagating in the z direction, and a weak spinning beam, circularly polarized in the yz plane and propagating along the x direction. The tweezers field exerts a conservative restoring torque on the dumbbell, which aligns its long axis in the x direction and creates two libration modes around this equilibrium. In contrast, the circularly polarized beam generates a non-conservative torque, which drives the dumbbell into a spinning motion around its long axis. This torque arises from the optical spin [29, 30] carried by the beam together with absorption or imperfect cylindrical symmetry of the dumbbell [31–33].

The rotational dynamics of the nanodumbbell [34] is thus governed by two libration angles φ and ϑ with respect to the x axis and the rotation angle ψ around its long axis. In the presence of friction and assuming small-angle libration, the dumbbell's spinning rate will accelerate until it reaches its steady-state value

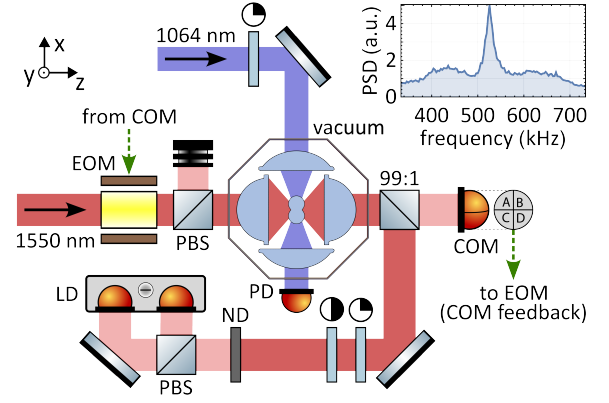


Figure 2. Experimental apparatus for spinning a dumbbell. The x polarized optical tweezers (wavelength 1550 nm) trap a dumbbell inside a vacuum chamber, while a circularly polarized beam (wavelength 1064 nm) propagating along x spins the dumbbell. Forward scattered light from the tweezers is split and subsequently sent to a quadrant photodiode and a balanced detector for center-of-mass (COM) and libration detection (LD), respectively. The detected COM motion is used to drive an electro-optic modulator (EOM) for feedback cooling x and y COM motion. The power of the spinning beam is monitored on a photodiode (PD). Inset: power spectral density (PSD, plotted in arbitrary units) of the libration motion of a trapped dumbbell recorded at a pressure of 0.1 mbar and without the spinning beam.

$\dot{\psi}_0 = \tau/(I_3\gamma_3)$ [1, 2, 4], where τ is the magnitude of the non-conservative torque, I_3 is the moment of inertia along the long axis, and γ_3 is the friction coefficient. The spinning motion reveals itself as a coupling $g = (I_3/2I_1)\dot{\psi}_0$ between the otherwise independent and harmonic libration modes, where I_1 is the moment of inertia along one short axis. The coupling leads to hybrid modes with eigenfrequencies

$$\Omega_{1/2} = \sqrt{\Omega_0^2 + g^2} \pm g, \quad (1)$$

where Ω_0 is the natural libration frequency [13]. The higher frequency Ω_1 corresponds to nutation of the long axis, whereas the lower frequency Ω_2 is associated with precession of the long axis around the x direction [35].

Most importantly, since the coupling rate $g = \tau/(2I_1\gamma_3)$ is directly related to the torque and friction, with the torque scaling linearly with the spinning beam power [34], in our experimental implementation we can control the coupling via the optical power of the circularly polarized spinning beam and the chamber pressure. For high enough spinning rates, we can push our system far into the deep-strong coupling regime, i.e., $g \gg \Omega_0$. In this regime we can approximate the eigenfrequencies as

$$\Omega_1 = 2g, \quad (2a)$$

$$\Omega_2 = \frac{\Omega_0^2}{2g}. \quad (2b)$$

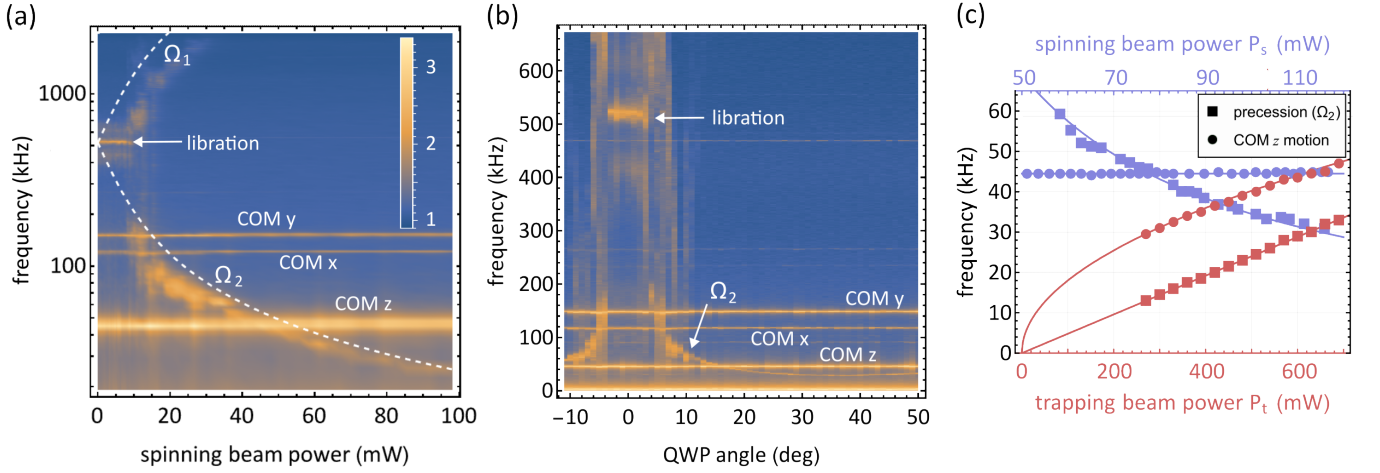


Figure 3. Measured effects of spinning on the libration power spectral density (PSD). Color in plots (a) and (b) shows $\log(\text{PSD})$ in arbitrary units. Measurements (a)-(c) were performed at a pressure of 10^{-3} mbar. (a): Measured PSDs as a function of the spinning beam power. As we increase the spinning beam power the libration peak splits into the high frequency (Ω_1) nutation mode and low frequency (Ω_2) precession mode, which are separated by $2g$. Fits to Eq. (1) are shown as white dashed lines. (b): Measured PSDs for different polarizations of the spinning beam with optical power of 100 mW. As the quarter-wave plate (QWP) angle is adjusted from 0° to 45° , the spinning beam polarization changes from linear to circular, and instead of the libration spectrum we observe the precession mode with frequency Ω_2 which dips below the COM z frequency. (c): Precession frequency Ω_2 and COM z motion frequency as a function of trapping beam power (with a 100 mW circularly polarized spinning beam) and as a function of spinning beam power (with a 700 mW trapping beam). Fits to Eq. (2b) are shown as solid lines.

As we increase the spinning rate of the dumbbell, the amplitude of nutation relative to precession decreases, and the motion becomes dominated by slow precession with frequency Ω_2 [36]. At the same time, the value of Ω_2 depends only weakly on g for high spinning rates.

EXPERIMENTAL SETUP.

In our experiment, depicted schematically in Fig. 2, silica nanodumbbells composed of two spherical nanoparticles (nominal diameter 143 nm) are optically trapped inside a vacuum chamber. The tweezers beam forming the trap (wavelength 1550 nm, power 700 mW) is focused with an $\text{NA} = 0.8$ lens. The light scattered by the particle is subsequently collected by an $\text{NA} = 0.7$ lens and analyzed to detect libration in the xy plane and the center-of-mass (COM) degrees of freedom. For detecting the COM motion we use a quadrant photodiode, while libration is recorded with the help of a balanced detector as in [6]. In order to stabilize the position of the dumbbell inside the trap, we cool the x and y COM motion at pressures below 10^{-4} mbar by parametric feedback [37]. The cooling is realized using an electro-optic modulator (EOM), which modulates the tweezers' power at twice the x and y COM frequencies [37].

We identify a trapped particle as a dumbbell when its COM x -to- y gas damping ratio is in the 1.1 – 1.15 range [2]. Another characteristic of dumbbells is their libration spectrum, which consists of a sharp libration peak at 525(3) kHz flanked by broad shoulders, as shown

by the inset of Fig. 2. This spectral shape originates from coupling between the libration modes introduced by thermally driven spinning around the long axis [5, 6, 13, 38].

The spinning beam (wavelength 1064 nm, tunable power up to 120 mW) is focused onto the dumbbell by an $\text{NA} = 0.3$ lens with 7.5 mm focal length. The beam is then collected by another $\text{NA} = 0.3$ lens and its power is monitored using a photodiode. The polarization state of the spinning beam is controlled by a quarter-wave plate (QWP). Due to its low power and weak focusing, the spinning beam does not significantly alter the libration potential [34].

RESULTS.

Figure 3(a) shows the measured libration spectra for different optical powers of the circularly polarized spinning beam at 10^{-3} mbar. For powers below 10 mW the thermally-driven spinning dominates, as evidenced by the constant libration frequency accompanied by the shoulder-like lineshape on both sides (cf. inset in Fig. 2). As we increase the spinning beam power above the 10 mW threshold, the libration mode splits into two hybrid modes created by the spinning motion. The white dashed curves are theoretical fits according to Eq. (1) and agree well with the experimental observations. We observe a broad high frequency nutation peak (Ω_1) and a narrow low frequency precession mode (Ω_2). As expected, the frequency Ω_1 of the nutation

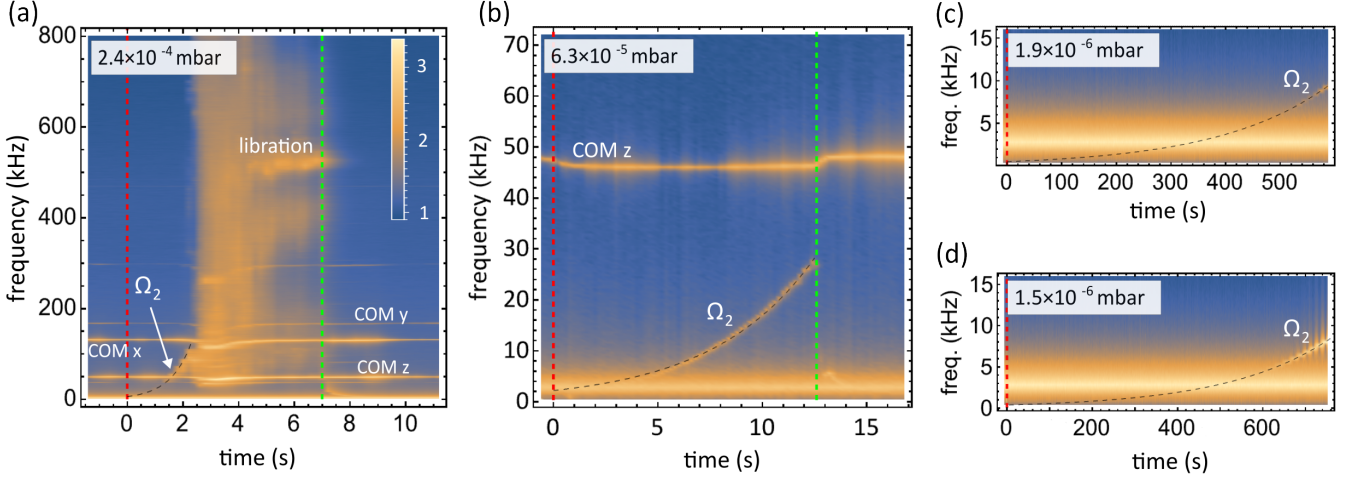


Figure 4. Ringdown measurements at different pressures. Each subfigure shows PSDs measured by the libration detector as a function of time t , after blocking the spinning beam (power 50 mW) at $t = 0$ marked by a dashed red line. The nanodumbbell’s spinning rate decreases due to friction, which is evidenced by the increase of the precession mode frequency Ω_2 . The time the spinning beam is switched back on is indicated in subfigures (a) and (b) by a dashed green line. Color in all plots shows $\log(\text{PSD})$ in arbitrary units. Black dashed lines are the fitted precession mode frequency, according to Eq. (3). **(a)**: Measurement at 2.4×10^{-4} mbar, without parametric feedback cooling of the COM. After approximately 4 s the dumbbell stops spinning and the libration peak appears. **(b)-(d)**: Measurement with parametric feedback cooling of the COM x and y motion at 6.3×10^{-5} mbar, 1.9×10^{-6} mbar, and 1.5×10^{-6} mbar, respectively. With decreasing pressure, the timescale for slowing down the free but damped spinning motion increases and the precession mode starts to become visible at later times. **(d)**: After this particular experiment the particle is lost at around 800 s.

mode increases and its amplitude decreases [36] with increasing spinning beam power. For spinning beam powers below 40 mW our measurements deviate from the theoretical model, which we ascribe to thermal and pressure-induced fluctuations, coupling to COM motion, and to deviations of the dumbbell from perfect cylindrical symmetry. However, we obtain very good agreement for spinning beam powers above 40 mW, where the spinning rate of the dumbbell transitions into the fast spinning regime characterized by $g \gg \Omega_0$ [see also Fig. 3(c)].

The torque τ experienced by the dumbbell can also be controlled by the polarization of the spinning beam. In Fig. 3(b) we show the measured libration spectra as a function of the QWP angle that changes the polarization of the spinning beam from linear to circular (see Fig. 2). When the QWP is set at 0° , the beam is linearly polarized in the z direction and has no detectable effect on the libration dynamics due to lack of optical spin. The coupling is dominated by thermally driven spinning, as if the spinning beam was absent. However, when the polarization becomes elliptical (QWP is rotated by approx. 5 degrees in either direction) the dynamics transitions abruptly into consistent spinning, as evidenced by the emerging low frequency precession mode (Ω_2). For circular polarization (around 45°), Ω_2 decreases clearly below the COM z frequency visible at 45 kHz.

Finally, we investigate the dependence of the precession frequency Ω_2 on the trapping beam power P_t and

the spinning beam power P_s in the fast spinning regime ($g \gg \Omega_0$). The natural libration frequency Ω_0 was shown to depend on the square root of P_t [13]. This implies, according to Eq. (2b), that the precession frequency Ω_2 depends linearly on P_t , as long as the coupling rate g is not affected by the trapping beam. The expected behavior is indeed confirmed by our measurements shown in Fig. 3(c). On the other hand, since the torque τ exerted on the dumbbell depends linearly on the spinning power P_s we expect, according to Eq. (2b), that Ω_2 scales inversely with P_s . We compare the behaviour of Ω_2 with that of the eigenfrequency of the COM z mode (which is expected to follow a square-root behavior on P_t and remain unaffected by changes in the spinning beam power P_s). The measured Ω_2 and COM z frequencies shown in Fig. 3(c) agree well with their respective predicted behaviors. We therefore conclude that Eq. (2b) correctly predicts the precession frequency in the fast spinning regime where $g \gg \Omega_0$. Note that the coupling strength surpasses the natural libration frequency even for moderate P_s . This is evidenced by the data in Fig. 3(c), which shows that the precession frequency Ω_2 decreases to 30 kHz for $P_s \approx 100$ mW. According to Eq. (2b), this corresponds to a coupling rate $g = 2\pi \times 4.6$ MHz. Assuming our dumbbells have a length-to-diameter ratio of 1.8 (as in Ref. [31]), we can estimate $I_3/I_1 \approx 0.6$, which yields a spinning rate of $\psi_0 \approx 2\pi \times 15$ MHz.

RINGDOWN MEASUREMENTS.

The steady-state spinning rate $\dot{\psi}_0 = \tau/(I_3\gamma_3)$ is inversely proportional to the damping rate γ_3 , which in turn is proportional to the gas pressure. Thus, controlling the pressure allows us to tune $\dot{\psi}_0$ over several orders of magnitude. As described before, we can infer the dumbbell's spinning rate from the measured hybrid mode frequencies. However, in practice we are only able to detect the precession mode Ω_2 for spinning rates up to $\dot{\psi}_0 \approx 30$ MHz. The reason for this is two-fold: first, as $\Omega_2/(2\pi)$ decreases below 3 kHz it becomes obscured by electronic noise in our detection system; second, large spinning rates lead to large angular momenta which stabilize the system and reduce the precession amplitude which results in poor signal-to-noise in our measurements [34]. We circumvent this problem by performing ringdown measurements by setting P_s to zero and observing the slowing down of the dumbbell's spinning rate [1]. Once the spinning rate approaches zero thermal fluctuations become dominant and the ringdown is a stochastic trajectory. However, for sufficiently high spinning rates thermal fluctuations can be ignored and the ringdown turns into a deterministic trajectory described by $\dot{\psi}(t) = \dot{\psi}(0)e^{-\gamma_3 t}$. Consequently, according to Eq. (2b), the precession frequency exponentially increases in time as:

$$\Omega_2(t) = \frac{\Omega_0^2}{g(0)} e^{\gamma_3 t}. \quad (3)$$

Note that this description is only valid when $g \gg \Omega_0$, and thus we only use Eq. (3) to determine $g(0)$ and γ_3 in this parameter regime.

Figure 4(a) shows a ringdown measurement performed at a pressure of 2.4×10^{-4} mbar. The spinning beam is switched off at $t = 0$ (red dashed line) and the dumbbell's spinning slows down until it reaches the thermally-driven regime at $t = 4$ s where the libration motion becomes visible. The beam is switched back on after approximately 7 s (green dashed line) and the random thermal motion gives way to the controlled spinning again. We fit the data with Eq. (3) (black dashed line) for times up to 2.2 s and observe that Ω_2 increases exponentially as expected. We present the obtained damping and coupling rate together with the spinning rate in Table I.

At pressures below 10^{-4} mbar we parametrically feed-back cool the x and y COM modes for stabilizing the particle's position in the trap to avoid particle loss. As an example, we show a ringdown measurement at 6.3×10^{-5} mbar in Fig. 4(b). The cooling is performed by modulating the trapping beam at twice the COM x and y frequencies [37]. The spinning beam is switched back on at $t \approx 12.5$ s, before Ω_2 reaches the COM z frequency. The data again show that Ω_2 increases exponentially after switching off the spinning beam, but the increase is slower than in Fig. 4(a) because of the lower pressure. Note that Ω_2 is only discernible from 4 s onwards, where

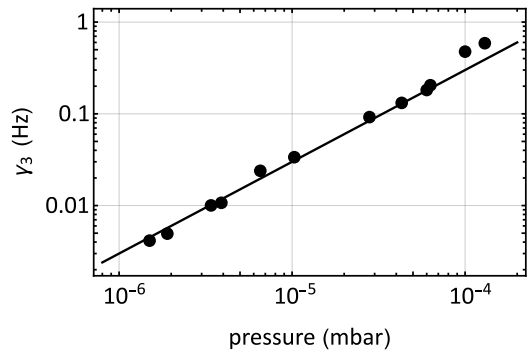


Figure 5. Damping rate γ_3 as a function of pressure extracted from ringdown measurements. The solid line is a linear fit (forced through the origin).

it emerges from the low frequency noise. Using this method we can measure high values of g , even when Ω_2 is not detectable in steady-state, i.e., when the spinning beam is continuously on.

We repeated similar measurements for even lower pressures [see Figs. 4(c) and (d)], down to 1.5×10^{-6} mbar, where we reached the exceptionally high coupling rate of $g(0)/\Omega_0 = 724(33)$, corresponding to a spinning rate of $\dot{\psi}(0) = 2\pi \times 1.20(6)$ GHz. Notably, these low pressure ringdown measurements require a slowing down period of several hundred seconds for the precession mode frequency to become detectable [see Figs. 4(c) and (d)]. This delay is a consequence of the damping rate γ_3 decreasing to values below 10 mHz and the spinning rate $\dot{\psi}(0)$ entering the GHz regime.

In Fig. 5 we plot our measurements of the damping rate γ_3 for different pressures together with a linear fit. According to theory, the damping of a symmetric rotor spinning along its long axis is proportional to a temperature-dependent accommodation coefficient as well as the gas density [39]. Our measurements indicate that the accommodation coefficient remains constant in the pressure range between 10^{-6} and 10^{-3} mbar, implying that the internal temperature of the dumbbell remains constant in this pressure range.

CONCLUSIONS.

We have demonstrated, for the first time, controlled spinning of an optically levitated nanodumbbell around its long axis. We achieve rotational rates exceeding $2\pi \times 1$ GHz. The long axis spinning couples the two libration modes and the coupling rate is shown to be 724 times larger than the natural libration frequency. This demonstration is an important step towards the development of levitated gyroscopes. The GHz spinning rate demonstrated in this work translates into a thermally limited gyroscope sensitivity (angular random walk) of $\Omega_{\text{ARW}} = \sqrt{4k_B T \gamma} / (\sqrt{I_3} \dot{\psi}_0) \approx 4 \times 10^{-6}$ rad/s/ $\sqrt{\text{Hz}}$ for current experimental parameters [40]. This is only two

Fig. 4	p_{gas} (mbar)	γ_3 (Hz)	$g(0)/(2\pi)$ (MHz)	$\dot{\psi}(0)/(2\pi)$ (MHz)	$g(0)/\Omega_0$
(a)	2.4×10^{-4}	$7.69(6) \times 10^{-1}$	2.25(25)	7.5(8)	4.29(48)
(b)	6.3×10^{-5}	$2.045(29) \times 10^{-1}$	63(2)	210(7)	120(4)
(c)	1.9×10^{-6}	$4.95(6) \times 10^{-3}$	268(10)	893(33)	510(19)
(d)	1.5×10^{-6}	$4.149(6) \times 10^{-3}$	380(17)	1267(58)	724(33)

Table I. Results of the ringdown measurements shown in Fig. 4.

orders of magnitude larger than the self-noise of the best high-end commercially available gyroscopes [41]. Moreover, our experiment can be further optimized, e.g., by using larger dumbbells ($\Omega_{\text{ARW}} \propto r^{-5/2}$, where r is the nanoparticle radius) or by lowering the pressure below 10^{-6} mbar.

Recent advances [1–9, 11–13, 33, 42] have brought rotational levitodynamics close to the quantum regime [14, 43]. The deep-strong coupling regime shown in our work is an important step for realizing quantum correlations between ground-state cooled libration modes, as ground states of such strongly coupled systems are intrinsically entangled and contain virtual excitations [44]. Our work further expands the potential that rotational degrees

of freedom offer for the creation and measurement of macroscopic quantum states [14, 24, 45].

The authors would like to thank C. Gonzalez-Ballester, J. Harris and the members of the Photonics Laboratory for fruitful discussions. This research was supported by the European Union’s Horizon 2020 research and innovation programme under grant agreement No. [863132] (IQLev), as well as the ETH Grant No. ETH-47 20-2. A. Norrman acknowledges support from the Research Council of Finland (Grant Nos. 354918 and 320166). F. van der Laan was supported by the Netherlands Organisation for Scientific Research (NWO).

-
- [1] R. Reimann, M. Doderer, E. Hebestreit, R. Diehl, M. Frimmer, D. Windey, F. Tebbenjohanns, and L. Novotny, Ghz rotation of an optically trapped nanoparticle in vacuum, *Phys. Rev. Lett.* **121**, 033602 (2018).
 - [2] J. Ahn, Z. Xu, J. Bang, Y.-H. Deng, T. M. Hoang, Q. Han, R.-M. Ma, and T. Li, Optically levitated nanodumbbell torsion balance and ghz nanomechanical rotor, *Phys. Rev. Lett.* **121**, 033603 (2018).
 - [3] J. Ahn, Z. Xu, J. Bang, P. Ju, X. Gao, and T. Li, Ultrasensitive torque detection with an optically levitated nanorotor, *Nat. Nanotechnol.* **15**, 89 (2020).
 - [4] F. van der Laan, R. Reimann, A. Militaru, F. Tebbenjohanns, D. Windey, M. Frimmer, and L. Novotny, Optically levitated rotor at its thermal limit of frequency stability, *Phys. Rev. A* **102**, 013505 (2020).
 - [5] J. Bang, T. Seberson, P. Ju, J. Ahn, Z. Xu, X. Gao, F. Robicheaux, and T. Li, Five-dimensional cooling and nonlinear dynamics of an optically levitated nanodumbbell, *Phys. Rev. Res.* **2**, 043054 (2020).
 - [6] F. van der Laan, F. Tebbenjohanns, R. Reimann, J. Vijayan, L. Novotny, and M. Frimmer, Sub-kelvin feedback cooling and heating dynamics of an optically levitated libration, *Phys. Rev. Lett.* **127**, 123605 (2021).
 - [7] J. Schäfer, H. Rudolph, K. Hornberger, and B. A. Stickler, Cooling nanorotors by elliptic coherent scattering, *Phys. Rev. Lett.* **126**, 163603 (2021).
 - [8] A. Pontin, H. Fu, M. Toroš, T. S. Monteiro, and P. F. Barker, Simultaneous cavity cooling of all six degrees of freedom of a levitated nanoparticle, *Nature Physics* **19**, 1003 (2023).
 - [9] Z. Xu and T. Li, Detecting casimir torque with an optically levitated nanorod, *Phys. Rev. A* **96**, 033843 (2017).
 - [10] S. Kuhn, B. A. Stickler, A. Kosloff, F. Patolsky, K. Hornberger, M. Arndt, and J. Millen, Optically driven ultra-stable nanomechanical rotor, *Nat. Commun.* **8**, 1670 (2017).
 - [11] M. Rashid, M. Toroš, A. Setter, and H. Ulbricht, Precession motion in levitated optomechanics, *Phys. Rev. Lett.* **121**, 253601 (2018).
 - [12] P. Ju, Y. Jin, K. Shen, Y. Duan, Z. Xu, X. Gao, X. Ni, and T. Li, Near-field ghz rotation and sensing with an optically levitated nanodumbbell (2023), [arXiv:2301.10868 \[quant-ph\]](https://arxiv.org/abs/2301.10868).
 - [13] T. Seberson and F. Robicheaux, Parametric feedback cooling of rigid body nanodumbbells in levitated optomechanics, *Phys. Rev. A* **99**, 013821 (2019).
 - [14] B. Stickler, K. Hornberger, and M. Kim, Quantum rotations of nanoparticles, *Nat. Rev. Phys.* **3**, 589–597 (2021).
 - [15] L. Magrini, R. A. Norte, R. Riedinger, I. Marinković, D. Grass, U. Delić, S. Gröblacher, S. Hong, and M. Aspelmeyer, Near-field coupling of a levitated nanoparticle to a photonic crystal cavity, *Optica* **5**, 1597 (2018).
 - [16] A. de los Ríos Sommer, N. Meyer, and R. Quidant, Strong optomechanical coupling at room temperature by coherent scattering, *Nature Communications* **12**, 276 (2021).
 - [17] J. Rieser, M. A. Ciampini, H. Rudolph, N. Kiesel, K. Hornberger, B. A. Stickler, M. Aspelmeyer, and U. Delić, Tunable light-induced dipole-dipole interaction between optically levitated nanoparticles, *Science* **377**, 987 (2022), <https://www.science.org/doi/pdf/10.1126/science.abp9941>.

- [18] K. Dare, J. J. Hansen, I. Coroli, A. Johnson, M. Aspelmeyer, and U. Delić, Linear ultrastrong optomechanical interaction (2023), [arXiv:2305.16226 \[quant-ph\]](#).
- [19] H. Rudolph, U. Delić, K. Hornberger, and B. A. Stickler, Quantum theory of non-hermitian optical binding between nanoparticles (2023), [arXiv:2306.11893 \[quant-ph\]](#).
- [20] D. Vitali, S. Gigan, A. Ferreira, H. R. Böhm, P. Tombesi, A. Guerreiro, V. Vedral, A. Zeilinger, and M. Aspelmeyer, Optomechanical entanglement between a movable mirror and a cavity field, *Phys. Rev. Lett.* **98**, 030405 (2007).
- [21] G. A. Peterson, S. Kotler, F. Lecocq, K. Cicak, X. Y. Jin, R. W. Simmonds, J. Aumentado, and J. D. Teufel, Ultrastrong Parametric Coupling between a Superconducting Cavity and a Mechanical Resonator, *Physical Review Letters* **123**, 247701 (2019).
- [22] J. Koch, G. R. Hunanyan, T. Ockenfels, E. Rico, E. Solano, and M. Weitz, Quantum Rabi dynamics of trapped atoms far in the deep strong coupling regime, *Nature Communications* **14**, 954 (2023).
- [23] C. P. Koch, M. Lemesko, and D. Sugny, Quantum control of molecular rotation, *Rev. Mod. Phys.* **91**, 035005 (2019).
- [24] B. A. Stickler, B. Papendell, S. Kuhn, B. Schirnski, J. Millen, M. Arndt, and K. Hornberger, Probing macroscopic quantum superpositions with nanorotors, *New J. Phys.* **20**, 122001 (2018).
- [25] K. Usami, Quantum-noise-limited angular momentum measurement for a micron-sized dielectric object (2007), [arXiv:0712.4303 \[quant-ph\]](#).
- [26] F. Tebbenjohanns, A. Militaru, A. Norrman, F. van der Laan, L. Novotny, and M. Frimmer, Optimal orientation detection of an anisotropic dipolar scatterer, *Phys. Rev. A* **105**, 053504 (2022).
- [27] A. Norrman, A. T. Friberg, J. J. Gil, and T. Setälä, Dimensionality of random light fields, *J. Eur. Opt. Soc.-Rapid Publ.* **13**, 36 (2017).
- [28] M. A. Alonso, Geometric descriptions for the polarization of nonparaxial light: a tutorial, *Adv. Opt. Photonics* **15**, 176 (2023).
- [29] K. Y. Bliokh and F. Nori, Transverse and longitudinal angular momenta of light, *Phys. Rep.* **592**, 1 (2015).
- [30] J. J. Gil, A. Norrman, A. T. Friberg, and T. Setälä, Spin of random stationary light, *Phys. Rev. A* **107**, 053518 (2023).
- [31] L. Bellando, M. Kleine, Y. Amarouchene, M. Perrin, and Y. Louyer, Giant diffusion of nanomechanical rotors in a tilted washboard potential, *Phys. Rev. Lett.* **129**, 023602 (2022).
- [32] F. van der Laan, *Rotational Levitodynamics*, Ph.D. thesis, ETH Zurich (2022).
- [33] M. Kamba, R. Shimizu, and K. Aikawa, Nanoscale feedback control of six degrees of freedom of a near-sphere, [arXiv:2303.02831 \(2023\)](#).
- [34] See Methods for the detailed description of the coordinate system, and the theoretical model of precession.
- [35] L. D. Landau and E. M. Lifshitz, *Mechanics, Third Edition: Volume 1 (Course of Theoretical Physics)*, 3rd ed. (Butterworth-Heinemann, 1976).
- [36] H. Goldstein, C. Poole, and J. Safko, *Classical Mechanics*, 3rd ed. (Pearson Education, 2001).
- [37] J. Gieseler, B. Deutsch, R. Quidant, and L. Novotny, Subkelvin Parametric Feedback Cooling of a Laser-Trapped Nanoparticle, *Physical Review Letters* **109**, 103603 (2012).
- [38] J. A. Zielińska, F. van der Laan, A. Norrman, M. Rimlinger, R. Reimann, L. Novotny, and M. Frimmer, Controlling optomechanical libration with the degree of polarization, *Phys. Rev. Lett.* **130**, 203603 (2023).
- [39] L. Martinetz, K. Hornberger, and B. A. Stickler, Gas-induced friction and diffusion of rigid rotors, *Phys. Rev. E* **97**, 052112 (2018).
- [40] K. Poletkin, Mechanical thermal noise in levitation micro-gyroscopes, in *Levitation Micro-Systems: Applications to Sensors and Actuators* (Springer International Publishing, Cham, 2021) pp. 135–154.
- [41] iXblue, [blueSeis-3A Portable rotational 3-component seismometer, absolute and broadband](#) (2022).
- [42] C. P. Blakemore, D. Martin, A. Fieguth, N. Priel, G. Venugopalan, A. Kawasaki, and G. Gratta, Librational feedback cooling, *Phys. Rev. A* **106**, 023503 (2022).
- [43] C. Gonzalez-Ballester, M. Aspelmeyer, L. Novotny, R. Quidant, and O. Romero-Isart, Levitodynamics: Levitation and control of microscopic objects in vacuum, *Science* **374**, eabg3027 (2021).
- [44] A. Frisk Kockum, A. Miranowicz, S. De Liberato, S. Savasta, and F. Nori, Ultrastrong coupling between light and matter, *Nature Reviews Physics* **1**, 19 (2019), 1807.11636.
- [45] Y. Ma, K. E. Khosla, B. A. Stickler, and M. S. Kim, Quantum persistent tennis racket dynamics of nanorotors, *Phys. Rev. Lett.* **125**, 053604 (2020).
- [46] E. W. Weisstein, Euler angles, [From MathWorld—A Wolfram Web Resource](#).
- [47] L. Novotny and B. Hecht, *Principles of Nano-Optics*, 2nd ed. (Cambridge University Press, 2012).
- [48] I. Toftul, G. Fedorovich, D. Kislov, K. Frizyuk, K. Koshelev, Y. Kivshar, and M. Petrov, Nonlinearity-induced optical torque, *Phys. Rev. Lett.* **130**, 243802 (2023).
- [49] R. Kitamura, L. Pilon, and M. Jonasz, Optical constants of silica glass from extreme ultraviolet to far infrared at near room temperature, *Appl. Opt.* **46**, 8118 (2007).
- [50] F. Monteiro, S. Ghosh, E. C. van Assendelft, and D. C. Moore, Optical rotation of levitated spheres in high vacuum, *Phys. Rev. A* **97**, 051802 (2018).
- [51] M. Schuck, D. Steinert, T. Nussbaumer, and J. W. Kolar, Ultrafast rotation of magnetically levitated macroscopic steel spheres, *Science Advances* **4**, e1701519 (2018), <https://www.science.org/doi/pdf/10.1126/sciadv.1701519>.
- [52] D. Hümmer, R. Lampert, K. Kustura, P. Maurer, C. Gonzalez-Ballester, and O. Romero-Isart, Acoustic and optical properties of a fast-spinning dielectric nanoparticle, *Phys. Rev. B* **101**, 205416 (2020).

METHODS

Particle description

In this work we focus on nanodumbbell particles, which are cylindrically symmetric objects comprised of two spheres attached to each other. We assume that the moment of inertia tensor as well as the real and imaginary parts of the polarizability tensor can be simultaneously diagonalized in the principal axes reference frame of the particle. We refer to this frame of reference as the "particle frame" and represent the principal axes by the unit vectors $(\mathbf{e}_1, \mathbf{e}_2, \mathbf{e}_3)$. We further let $\boldsymbol{\alpha}' = \text{diag}(\alpha'_1, \alpha'_1, \alpha'_3)$ and $\boldsymbol{\alpha}'' = \text{diag}(\alpha''_1, \alpha''_1, \alpha''_3)$ denote the real and imaginary parts of the static polarizability tensor of the object in the intrinsic body frame, respectively, assuming $\alpha'_1 < \alpha'_3$. The moment of inertia of the particle is described by the tensor $\mathbf{I} = \text{diag}(I_1, I_1, I_3)$, where we assume $I_1 > I_3$. We refer to \mathbf{e}_3 (the principal axis with the largest polarizability) as the "long axis" of the object.

In order to describe the orientation of the particle frame with respect to the laboratory frame (x, y, z) , we use the intrinsic x -convention of Euler angles denoted as ϕ , θ and ψ (see [46] and §35 in [35]). The Euler angles ϕ and θ describe the orientation of the long axis of the rotor. In turn, the Euler angle ψ describes rotation of the nanodumbbell around its long axis, i.e., $\dot{\psi}$ is the spinning speed. The angle measured in the experiment is ϕ , which corresponds to the orientation of the long axis in the xy plane with respect to the y axis.

In order to transform a vector from the laboratory to the particle frame we first rotate it by the angle ϕ around z , then by θ around \mathbf{e}_1 and finally by ψ around \mathbf{e}_3 . The transformation matrix \mathbf{R} corresponding to these three rotation operations is given in [46].

Conservative torques

In this section we calculate the potential arising from the real part $\boldsymbol{\alpha}'$ of the polarizability tensor of the particle. The libration dynamics is dictated by the direction of the electric dipole moment induced by the optical field, whose orientation depends on the particle orientation and in general is not parallel to the electric field.

We describe the electric field of the linearly polarized trapping beam at the tweezers focal point as $\mathbf{E}_t = (E_t e^{i\omega_t t}, 0, 0)^T$. In turn, we can write the electric field of the spinning beam (also at the tweezers focal point) as $\mathbf{E}_s = (0, E_s e^{i\omega_s t}, iE_s e^{i\omega_s t})^T$. The dipole moment induced on the trapped anisotropic particle, expressed in the laboratory frame, is given by

$$\mathbf{p} = \mathbf{R}^{-1} \boldsymbol{\alpha}' \mathbf{R} \mathbf{E}, \quad (4)$$

where $\mathbf{E} = \mathbf{E}_t + \mathbf{E}_s$ is also expressed in the laboratory reference frame. Since in general \mathbf{p} and \mathbf{E} are not parallel, the potential energy U associated with the orientation of

the particle (after averaging over optical frequencies) is

$$U = -\frac{1}{4} \text{Re}(\mathbf{p} \cdot \mathbf{E}^*). \quad (5)$$

Due to the fact that the trapping and spinning fields oscillate at different optical frequencies ω_t and ω_s , corresponding to their respective wavelengths $\lambda_t = 1550$ nm and $\lambda_s = 1064$ nm, we can average out the cross terms oscillating at $\omega_s - \omega_t$ and calculate the potential components arising from both components independently. The potential arising from the trapping beam then reads

$$U_t = -\frac{1}{4} E_t^2 (\alpha'_1 + \Delta\alpha' \sin^2 \phi \sin^2 \theta), \quad (6)$$

where $\Delta\alpha' = \alpha'_3 - \alpha'_1$. The term U_t aligns the long axis of the particle with the trapping beam electric field, which points along x axis. The potential arising from the spinning beam is

$$U_s = -\frac{1}{4} E_s^2 (\alpha'_1 + \alpha'_3 - \Delta\alpha' \sin^2 \phi \sin^2 \theta). \quad (7)$$

In turn, the potential term U_s tries to align the long axis of the particle to the yz plane, thus counteracting U_t . However, since the trapping field is much stronger than the spinning beam, $|E_t|^2 \gg |E_s|^2$, we can approximate the total potential as $U \approx U_t$.

The long axis of the dumbbell oscillates in the potential minimum, occurring for $\phi = \theta = \pi/2$, which gives rise to two libration modes $\vartheta = \theta - \pi/2$ and $\varphi = \phi - \pi/2$. Expanding the potential around minimum and removing orientation-independent terms leads to

$$U \approx \frac{1}{2} I_1 \Omega_0^2 (\varphi^2 + \vartheta^2), \quad (8)$$

where $\Omega_0 = \sqrt{\Delta\alpha' E_t^2 / 2I_1}$ denotes the libration frequency.

Finally, let us describe the libration dynamics due to the potential U in terms of the restoring torque $\boldsymbol{\kappa}$, whose components in the particle frame read

$$\kappa_1 = -I_1 \Omega_0^2 (\vartheta \cos \psi + \varphi \sin \psi), \quad (9a)$$

$$\kappa_2 = -I_1 \Omega_0^2 (-\vartheta \sin \psi + \varphi \cos \psi), \quad (9b)$$

$$\kappa_3 = 0. \quad (9c)$$

Note that the restoring torque components in the particle frame of reference depend on angle ψ , describing the rotation of the particle around its long axis.

Non-conservative torque

The non-conservative dynamics in our experiment arises from the circular polarization of the spinning beam, which provides constant torque spinning the particle around its long axis. This torque can arise from optical absorption or scattering [31] and depends on the x component of the optical spin $S_x = \text{Im} \langle \mathbf{E}^* \times \mathbf{E} \rangle_x$ of the

focused electric field \mathbf{E} at the location of the dumbbell. The torque from absorption relies on the imaginary part of the dumbbell polarizability and is given by $\tau_{\text{abs}} = \frac{1}{2}\alpha_3'' S_x$.

Optical torque transfer by scattering requires some optical anisotropy that breaks the dumbbell's cylindrical symmetry. The scattering torque is given by $\tau_{\text{sc}} = \frac{1}{2}(\delta\alpha')^2 g S_x$ [31], where $\delta\alpha'$ is a measure for the optical anisotropy and $g = \omega^3/(6\pi\epsilon_0 c^3)$. This anisotropy could arise from a deviation from the perfectly spherical shape of the two particles constituting the dumbbell [33].

Regardless of the mechanism of the angular momentum transfer from the light to the particle, we describe the effect of the circularly polarized spinning beam propagating along x as a constant torque $\boldsymbol{\tau} = (\tau, 0, 0)$ in the lab frame. We expect the torque magnitude to be proportional to the spinning beam power, in other words $\tau \propto |E_s|^2$. The components of $\boldsymbol{\tau}$ in the particle frame read:

$$\tau_1 = (-\varphi \cos \psi + \vartheta \sin \psi)\tau, \quad (10a)$$

$$\tau_2 = (\vartheta \cos \psi + \varphi \sin \psi)\tau, \quad (10b)$$

$$\tau_3 = \tau, \quad (10c)$$

where we have expanded to the first order around the particle orientation in the potential minimum (set by the trapping beam).

Therefore, the total torque \mathbf{K} experience by our particle, which includes both the conservative torque arising from the potential U and non-conservative spinning torque $\boldsymbol{\tau}$ amounts to

$$K_1 = \tau_1 + \kappa_1 \approx -I_1\Omega_0^2(\vartheta \cos \psi + \varphi \sin \psi), \quad (11a)$$

$$K_2 = \tau_2 + \kappa_2 \approx -I_1\Omega_0^2(-\vartheta \sin \psi + \varphi \cos \psi), \quad (11b)$$

$$K_3 = \tau_3 + \kappa_3 \approx \tau. \quad (11c)$$

when expressed in the particle frame of reference. We have neglected the terms τ_1 and τ_2 [see Eqs. (10a) and (10b)], which introduce a small coupling between libration modes φ and ϑ . This coupling has a negligible effect on the libration dynamics (dominated by the strong coupling introduced by the spinning motion), as $|E_s|^2 \ll |E_t|^2$ implies that $\tau \ll I_1\Omega_0^2$.

Equations of motion

This section contains the analysis of the Euler equations of motion in presence of the torque derived in the previous section. We begin by expressing the angular velocity ω in the particle frame and expanding it to the first order in libration angles φ and ϑ :

$$\omega_1 \approx \dot{\varphi} \sin \psi + \dot{\vartheta} \cos \psi, \quad (12a)$$

$$\omega_2 \approx \dot{\varphi} \cos \psi - \dot{\vartheta} \sin \psi, \quad (12b)$$

$$\omega_3 \approx -\dot{\varphi}\vartheta + \dot{\psi}. \quad (12c)$$

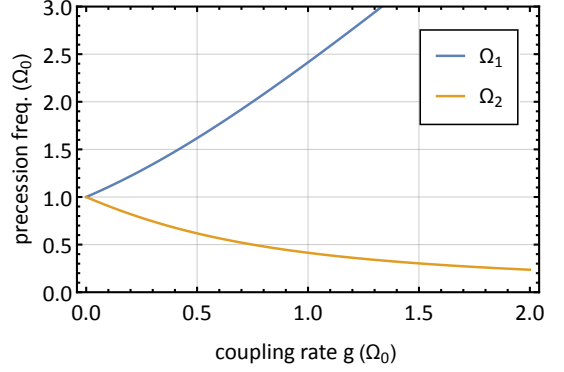


Figure 6. Precession modes Ω_1 and Ω_2 calculated from Eq. (1) in the units of natural libration frequency Ω_0 .

In the remainder of this work we are interested in the regime of large $\dot{\psi}$ and small-amplitude libration, therefore we further approximate the third component of the angular velocity as $\omega_3 \approx \dot{\psi}$.

Particle-frame Euler equations of motion for our cylindrically symmetrical dumbbell read:

$$K_1 = I_1\dot{\omega}_1 - \Delta I\omega_2\omega_3, \quad (13a)$$

$$K_2 = I_1\dot{\omega}_2 + \Delta I\omega_1\omega_3, \quad (13b)$$

$$K_3 = I_3\dot{\omega}_3, \quad (13c)$$

where $\Delta I = I_1 - I_3$. Using the expressions for torque (see Eqs. (11a)–(11c)) and angular velocity (see Eqs. (12a)–(12c)) components, we can rewrite Eqs. (13a)–(13c) as:

$$I_1\ddot{\vartheta} + I_3\dot{\varphi}\dot{\psi} = -I_1\Omega_0^2\vartheta, \quad (14a)$$

$$I_1\ddot{\varphi} - I_3\dot{\vartheta}\dot{\psi} = -I_1\Omega_0^2\varphi, \quad (14b)$$

$$I_3\ddot{\psi} = \tau. \quad (14c)$$

Note that Eqs. (14a) and (14b) describe two coupled harmonic oscillators ϑ and φ , whereas according the Eq. (14c), the velocity of the spinning around the long axis $\dot{\psi}$ increases to infinity. In order to avoid this problem, we have to expand the model to include friction in Eq. (14c). In presence of friction (described by coefficient γ_3), the spinning speed $\dot{\psi}$ will increase until it reaches a stationary value $\dot{\psi}_0 = \tau/(I_3\gamma_3)$, for which driving torque τ is balanced by the friction [1, 2].

Coupled libration modes

Let us now focus on the coupled libration modes described by Eqs. (14a) and (14b) and rewrite them explicitly introducing the coupling rate g ,

$$\ddot{\vartheta} + 2g\dot{\varphi} = -\Omega_0^2\vartheta, \quad (15a)$$

$$\ddot{\varphi} - 2g\dot{\vartheta} = -\Omega_0^2\varphi, \quad (15b)$$

where $g = (I_3/2I_1)\dot{\psi}_0$. In agreement with [13], the solution can be written as

$$\vartheta = \alpha_1 \cos(\Omega_1 t + \delta_1) + \alpha_2 \cos(\Omega_2 t + \delta_2), \quad (16a)$$

$$\varphi = \alpha_1 \sin(\Omega_1 t + \delta_1) - \alpha_2 \sin(\Omega_2 t + \delta_2) \quad (16b)$$

where $\alpha_{1/2}$ and $\delta_{1/2}$ depend on initial angular displacements and velocities and the eigenfrequencies read

$$\Omega_{1/2} = \sqrt{\Omega_0^2 + g^2} \pm g. \quad (17)$$

Note that the fast precession (nutation) mode with frequency Ω_1 corresponds to a circular motion of the long axis in the counterclockwise direction (for τ pointing along the positive x direction), and the slow precession mode corresponds to a clockwise long axis motion.

The dependence of $\Omega_{1/2}$ on the coupling rate g is shown in Fig. 6. For a fast spinning dumbbell ($g \gg \Omega_0$) the frequencies can be approximated as:

$$\Omega_1 = 2g, \quad (18a)$$

$$\Omega_2 = \frac{\Omega_0^2}{2g}. \quad (18b)$$

Finally, let us turn our attention to the amplitudes of precession and nutation. For a rapidly spinning top, the ratio between the amplitude of nutation α_1 and the amplitude of precession α_2 decreases proportionally to the spinning speed $\dot{\psi}$ squared [36]. Therefore we expect nutation will be negligible for a rapidly spinning dumbbell and the dynamics will be dominated by slow precession with frequency Ω_2 . The amplitude of the slow precession α_2 is equivalent to the tilt between the long axis of the dumbbell and x axis. This angle will stay almost constant as the dumbbell precesses, except for fast, small-amplitude oscillations caused by nutation. The effective potential governing the motion of the tilt angle α_2 can be written as $U_{\text{ef}} = \frac{1}{2}I_1(g^2 + \Omega_0^2)\alpha_2^2$ [35]. Applying equipartition theorem to this degree of freedom allows us to predict the average precession amplitude (tilt angle) of the thermally driven spinning top, which yields:

$$\langle \alpha_2^2 \rangle = \frac{k_B T}{I_1(\Omega_0^2 + g^2)} \quad (19)$$

Comparing the above result with Eq. 16b indicates that the oscillation amplitude of the libration angle φ measured in our experiment will behave similarly (if the angular degrees of freedom except ψ are in thermal equilibrium with the surrounding gas). To summarize, we expect that both the amplitude of the nutation and precession will diminish as we increase the spinning

speed, with nutation signal diminishing much faster. In practice, the amplitude of precession motion may be affected by misalignment between the spinning beam and the tweezers' polarization and external rotation of the experimental apparatus (e.g. due to the floating optical table).

The spinning torque

We estimate that the magnitude of the spin vector $\text{Im} \langle \mathbf{E}_s^* \times \mathbf{E}_s \rangle$ [30] carried by the spinning beam can reach up to $5 \times 10^{12} \text{ V}^2/\text{m}^2$. For comparison, the electric field squared corresponding to the trapping beam at the focal spot is 200 times larger. Additionally, it is interesting to compare the spin angular momentum carried by the spinning field to the transverse spin generated by focusing the linearly polarized trapping beam near the trapping region [38, 47]—in our experiment the angular momentum of the spinning beam is an order of magnitude smaller.

The damping rates γ_3 and the spinning rates extracted from the ringdown measurements (see main text) allow us to estimate the torque exerted on the dumbbell by a circularly polarized beam, arriving at $\tau = 5 \times 10^{-25} \text{ N m}$ for 100 mW of the optical power. We are unable to determine whether the torque arises from optical absorption, scattering (which requires breaking the cylindrical symmetry of the dumbbell) or other processes [48]. Attributing this torque to absorption requires the dumbbell's absorption coefficient to be two orders of magnitude larger than expected for bulk silica at 1064 nm [49]. On the other hand, attributing the torque to the scattering process [31], requires the polarizability of the dumbbell along the two short axes to differ by approximately 3%. Both increased absorption and imperfect spherical shape of the silica nanoparticles have been reported by other researchers [33, 50].

Particle deformation due to centrifugal forces

The calculated tensile stress generated by centrifugal force in silica nanodumbbells in our experiments reaches 0.5 GPa [1, 51]. The high spinning rates generate a tensile stress of 0.5 GPa [1, 51] and approach the regime of deforming the particle shape [52]. However, no consistent changes in characteristic frequencies and damping rates, temporary or permanent, were observed. We have recorded a single case of deformation (out of ~ 15 dumbbells investigated in total). After spinning with approx. 200 MHz, the particle's x -to- y gas damping ratio changed from 1.14 to 1.07, and the natural libration frequency decreased by 35%. The data obtained from this particle is not used in the manuscript.